Received 23 June 2021
Revised 25 October 2021
Accepted 26 November 2021

Multiobjective optimization of compensation networks for wireless power transfer systems

Manuele Bertoluzzo
Department of Industrial Engineering, University of Padova, Padova, Italy

Paolo Di Barba
Department of Electrical, Computer and Biomedical Engineering, University of Pavia, Pavia, Italy

Michele Forzan
Department of Industrial Engineering, University of Padova, Padova, Italy

Maria Evelina Mognaschi
Department of Electrical, Computer and Biomedical Engineering, University of Pavia, Pavia, Italy, and

Elisabetta Sieni
Department of Theoretical and Applied Sciences, University of Insubria, Varese, Italy

Abstract

Purpose – The purpose of this paper is to show how the EStra-Many method works on optimization problems characterized by high-dimensionality of the objective space. Moreover, a comparison with a more classical approach (a constrained bi-objective problem solved by means of NSGA-II) is done.

Design/methodology/approach – The six reactances of a compensation network (CN) for a wireless power transfer system (WPTS) are synthesized by means of an automated optimal design. In particular, an evolutionary algorithm EStra-Many coupled with a sorting strategy has been applied to an optimization problem with four objective functions (OFs). To assess the obtained results, a classical genetic algorithm NSGA-II has been run on a bi-objective problem, constrained by two functions, and the solutions have been analyzed and compared with the ones obtained by EStra-Many.

Findings – The proposed EStra-Many method identified a solution (CN synthesis) that enhances the WPTS, considering all the four OFs. In particular, to assess the synthesized CN, the Bode diagram of the frequency response and a circuital simulation were evaluated *a posteriori*; they showed good performance of the CN, with smooth response and without unwanted oscillations when fed by a square wave signal with offset. The EStra-Many method has been able to find a good solution among all the feasible solutions, showing potentiality also for other fields of research, in fact, a solution nondominated with respect to the starting point has been identified. From the methodological viewpoint, the main finding is a new formulation of the many-objective optimization problem based on the concept of degree of conflict, which gives rise to an implementation free from hierarchical weights.

COMPEL - The international journal for computation and mathematics in electrical and electronic engineering
Vol. 41 No. 2, 2022
pp. 674-689
Emerald Publishing Limited
0332-1649
DOI 10.1108/COMPEL-06-2021-0204

Originality/value – The new approach EStra-Many used in this paper showed to properly find an optimal solution, trading-off multiple objectives. The compensation network so synthesized by the proposed method showed good properties in terms of frequency response and robustness. The proposed method, able to deal effectively with four OFs, could be applied to solve problems with a higher number of OFs in a variety of applications because of its generality.

Keywords Wireless power transfer, Multiobjective optimization, Many-objective optimization, Wireless power transfer system, Compensation network synthesis

Paper type Research paper

1. Introduction

Wireless power transfer systems (WPTSs) operations rely on the inductive coupling between a transmitting and a receiving coil (Bi *et al.*, 2016; Campi *et al.*, 2020; Covic and Boys, 2013a, 2013b; Di Capua *et al.*, 2021; Feng *et al.*, 2018; Kindl *et al.*, 2020; Lukic and Pantic, 2013; Jha *et al.*, 2018; Choi *et al.*, 2015; Siqi and Mi, 2015). Suitable compensation networks (CNs) are connected to the coils to increase the power transferred to the load and the efficiency of the device (Bertoluzzo, Forzan, *et al.*, 2020; Chen *et al.*, 2020; Feng *et al.*, 2018; Villa *et al.*, 2012; Kindl *et al.*, 2020; Li *et al.*, 2015; Mohamed *et al.*, 2016; Pantic and Lukic, 2012; Qu *et al.*, 2017; Zhang and Mi, 2016). Optimization methods were used in the design of WPTSs and CNs for car supply (Cirimele *et al.*, 2018; Cruciani *et al.*, 2020a; Li *et al.*, 2018; Orasanu *et al.*, 2018; Winges *et al.*, 2019; Yakala *et al.*, 2021; Zhang and Mi, 2016) or to size the electromagnetic shield (Arduino *et al.*, 2020; Campi *et al.*, 2020; Cruciani *et al.*, 2020a, 2020b). The optimization of WPTS is largely explored to design the wireless recharge of other vehicles as e.g. electric railway (Lee *et al.*, 2014) or other electrical devices, as e.g. in Ali *et al.* (2019, 2020), Shen and Clerckx (2021) and Tan *et al.* (2019). In Chen *et al.* (2020), evolutionary algorithms were used to optimize CNs, whereas in Kindl *et al.* (2020) and Li *et al.* (2015, 2018), the improvement of the devices is based on the search for the best efficiency related to the load.

In Bertoluzzo *et al.* (2020), Bertoluzzo and Sieni (2019) authors presented automatic methods to design the reactances of generic CNs for automotive applications. In those papers, bi-objective, efficiency and power-to-load, the problem is solved. Usually, the CNs are designed considering only the nominal supply angular frequency ω_0; however, their impedance at higher and lower angular frequency ω must be high to filter out the high-frequency current-harmonics and to prevent the circulation of continuous-current components. The first of these occurrences arise because usually the WPTSs are supplied by a square wave modulated voltage that encompasses all the odd harmonics of the supply frequency; the second derives from the not ideal matching between the amplitude and the duty cycles of the positive and the negative semi periods of the supply voltage. From this background, a many-objective problem arises i.e. maximize the efficiency and the transferred power and maximize the impedance at $\omega_{100}=100\cdot\omega_0$ and $\omega_{0.01}=\omega_0/100$, where ω_{100} and $\omega_{0.01}$ are chosen as representative of the low and high-frequency bands, respectively. In this paper, to solve a many-objective problem with four objective functions (OFs), an algorithm presented by two of the authors in Di Barba *et al.* (2020) is applied. Results were

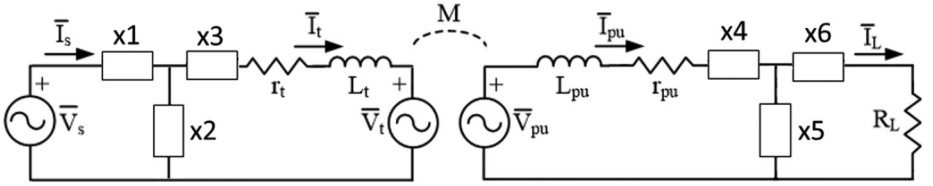

Figure 1.
Scheme of the WPTS with CN

compared with the ones found using a constrained-version of the NSGA-II algorithm (Deb, 2001; Lahanas *et al.*, 2003; Deb and Jain, 2014; Qingfu Zhang, 2009; D'Souza *et al.*, 2010).

2. The many-objective problem

Figure 1 shows the CN that connects the coupling inductances L_t and L_{pu} and the WPTS system to the power supply (left) and to the load (right). The power circuit works at 85 kHz, $\omega_{0,}$ as prescribed by the society of automotive engineers (SAE) regulation ("SAE J 2954 Wireless Power Transfer for Light-Duty Plug-in/Electric Vehicles and Alignment Methodology", n.d.). The considered CN has a T topology at both sides of the WPTS. In this problem, the CN is characterized by six design variables (x_1, x_2, x_3, x_4, x_5, x_6), i.e. the reactances of the CN components represented in Figure 1.

They can vary in the range [–500; 500] Ω: if the optimal value is positive, an inductance is identified; otherwise, it is a capacitance. Four OFs have been considered: function f_1 is the efficiency of the WPTS, η, function f_2 is the power transferred to the load, P_L. Because they were minimized, the following functions were considered in the optimization problem as follows:

$$f_1 = -\eta \tag{1}$$

$$f_2 = -P_L \tag{2}$$

In computing f_1 and f_2 the inductive reactances are modeled considering their inductance and an equivalent series-connected parasitic resistance (ESR). The ESRs cause unwanted losses in the CN and should be reduced as much as possible by adopting suitable technologies in building the inductive elements of the CN. In setting the many-objective problem, it is not possible to know in advance the actual values of the ESRs, and consequently, it has been hypothesized that the quality factor $Q = \omega_0 L/\text{ESR}$ of the inductive element is equal to 130, i.e. the same as the coupling coil available in the laboratory device, which has the parameters reported in Table 1.

During the optimization process, the ESRs of the inductive elements are adjusted to their optimized inductances to maintain the given Q for each of them.

The OFs f_3 and f_4 are expressed as follows:

$$f_3 = Z_{\omega 0}/Z_{\omega 100} \tag{3}$$

$$f_4 = Z_{\omega 0}/Z_{\omega 0.01} \tag{4}$$

where $Z_{\omega 0}$ is the impedance at the supply inverter output at the nominal supply angular frequency ω_0, and $Z_{\omega 100}$ and $Z_{\omega 0.01}$ are the impedances at the angular frequencies ω_{100} and $\omega_{0.001}$.

3. The optimization methods

3.1 The many-objective method

The idea behind this paper is to exploit a single-objective optimization algorithm for minimizing a suitable preference function, which takes into account all the OFs of the

Table 1. Parameters of the coupling inductances

L_t	120 μH
L_{pu}	120 μH
M	30 μH
Q	130
R_L	5.6 Ω

optimization problem. The chosen method is EStra, a lowest-order evolutionary algorithm, which has proven to be effective and reliable (Di Barba and Mognaschi, 2009).

Traditionally, preference functions are defined as weighted sums of individual objectives, and the choice of individual weights is the bias. In contrast, in the proposed method, the aim is to define a weight-free preference function, in view of this, the key idea is the degree of conflict among solutions because, in Pareto-like optimality, the nondominated solutions exhibit the lowest degree of conflict in the set of solutions.

Hence, the road map turns out to be as follows:

- define a preference function, modeling the degree of conflict among objectives, whatever the number of objectives;
- minimize the preference function by means of an evolution strategy algorithm, i.e. a derivative-free and global-optimum oriented algorithm; and
- identify a set of least-conflict solutions, approximating a Pareto-optimal set.

The core operation is to compute the degree of conflict between $m \geq 2$ OFs ($f_1, f_2, \ldots, f_m$) that are assumed to be simultaneously minimized. After sorting in ascending order, the rank of a solution is defined as the sorting index of the relevant OF values.

The computation of the degree of conflict of a solution, called score, is based on the sorting indices of the OFs; its computing procedure is shown in Figure 2.

Eventually, the goal is to minimize s with respect to any x in the design space Ω. In view of this, suppose that the preference function s has been linked with a zero-order optimization algorithm; whenever a new candidate solution is created by the algorithm, the set S is expanded by incorporating the $(n+1)$th solution (growing set scheme). The whole procedure is repeated up to convergence. For the algorithm to work, an initial set S_0 has to be supplied.

It has to be noted that the ranking value assigned to each solution is relevant to the current set S of solutions; whenever a new solution is added to or removed from the set S, the solution score of the individual solution has to be recomputed. Hence, the sorting (or ranking) operation of Figure 2 must be done at each iteration of the optimization, considering the current set of solutions S.

Specifically, the EStra method, a zero-order optimization algorithm, is chosen. If the method converged, it identified a single Pareto-optimal solution. The EStra method coupled with the sorting strategy explained above is called EStra-Many.

3.2 Constrained classical bi-objective method

To compare the results obtained by the EStra-Many method with a well-known and assessed method, the non-dominated sorting genetic algorithm (NSGA-II) is chosen. An interesting alternative to NSGA-II could be NSGA-III (Deb and Jain, 2014), which is more recent and able to deal with more than two OFs at the same time, on the other hand; however, NSGA-III does not seem to be so far as popular as NSGA-II, probably because of the need of providing reference solution points in the search space, which might be cumbersome for the user to provide.

In general, NSGA-II, the classical nondominated sorting genetic algorithm, developed by Deb (D'Souza *et al.*, 2010; Qingfu Zhang, 2009; Deb and Jain, 2014), is used to solve optimization problems from the multiobjective viewpoint, which means to approximate the whole Pareto front; however, the higher dimension of the objective space the less selective the Pareto front because there are very many in different solutions and so the classical criterion is loosely selective. In this paper, NSGA-II was used to optimize the efficiency of the WPTS and the power transferred to the load, f_1 and f_2, respectively, whereas f_3 and f_4 are considered as constraints. In practice, a threshold level for f_3 and f_4 was set, and for all the solutions with f_3 or f_4 larger than the prescribed threshold value, an out-of-range value for f_1 and f_2 is assigned. In

this respect, a penalty technique is applied for handling constraints. In practice, the solutions are discarded when not fulling the constraints. In the paper, depending on the considered case, different constraint levels were considered. In particular, the level was set between $1.5{\cdot}10^{-4}$ and 1 because in this problem, f_3 and f_4 must be lower than 1.

3.3 Classical multiobjective method

A further comparison between the proposed EStra-Many method and the classical multiobjective approach is carried out by means of NSGA-II applied to four OFs f_1, f_2, f_3 and f_4.

4. Optimization results

The optimization algorithm has been run for 700 iterations. Because EStra is a $1+1$ algorithm, one individual is processed at each run. The starting point and the improved solution are in Table 2.

NSGA-II method was run many times. In particular, the thresholds for f_3 and f_4 were different for each run: in general, the evolutionary algorithms have a poor behavior when constraints are handled, the threshold values have been tightened more and more at each run to make the constraints progressively more severe. In each run, 50 individuals and 250 generations are

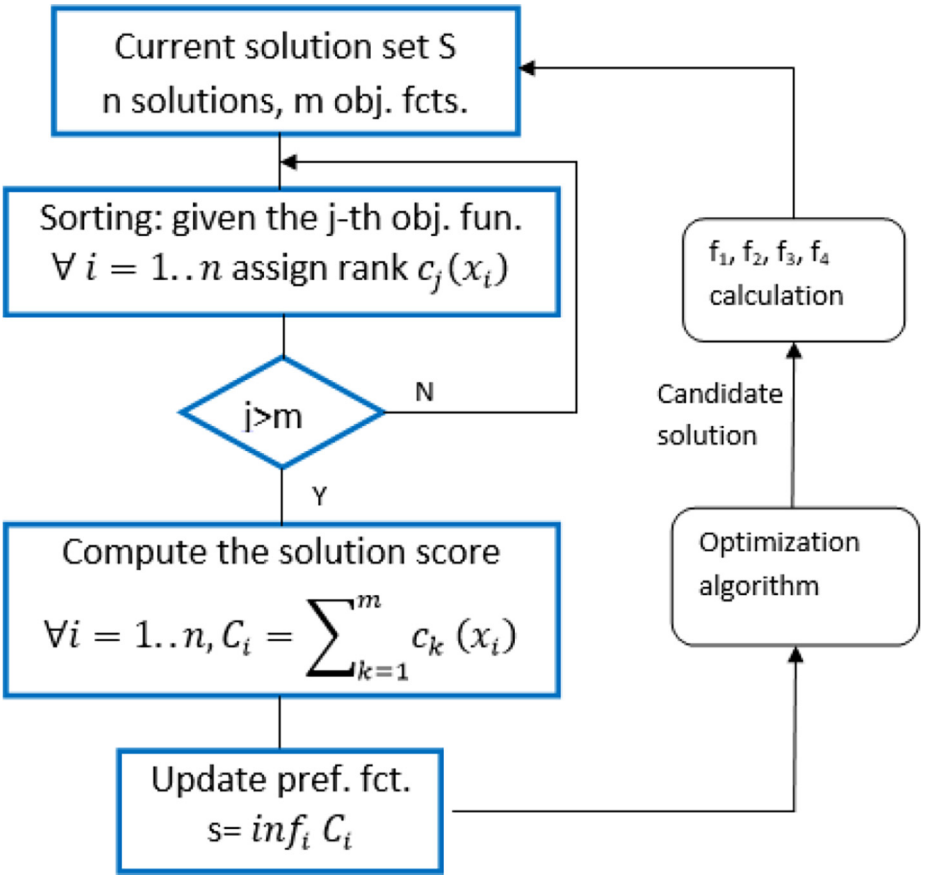

Figure 2.
Block diagram of the many-objective method; the sorting strategy

considered. The results are shown in Figure 3; elements highlighted with green point-down triangles represent the NSGA-II solutions with maximum transferred power, green point-up triangles denote the NSGA-II solutions with maximum efficiency, and red stars are relevant to the solutions chosen by the designer as a good trade-off between the values taken by the OFs.

Looking at Figure 3, it can be noted that the fronts found by NSGA-II are wider when the threshold of the constraints is higher; the lower the constraint values, the narrower the Pareto fronts (black triangles in Figure 3).

All these solutions are characterized by function f_3 equal to or higher than $1.68{\cdot}10^{-4}$ and f_4 higher than $1.5{\cdot}10^{-4}$. All in one, it can be noted that when the threshold values of f_3 and f_4 are comparable to the relevant values independently found by EStra-Many, then the front recovered by NSGA-II degenerates to a single solution point. The design variables and the

	x_1 [Ω]	x_2 [Ω]	x_3 [Ω]	x_4 [Ω]	x_5 [Ω]	x_6 [Ω]
Starting point	–69.7	223	–457	247	427	179
Final point	188	–380	–451	–57.2	–295	–22.4

	η [NU]	P [W]	$Z_{\omega 0}/Z_{\omega 100}$ (f_3 [NU])	$Z_{\omega 0}/Z_{\omega 0.01}$ (f_4 [NU])
Starting point	$6.32{\cdot}10^{-4}$	$1.61{\cdot}10^{-8}$	$9.05{\cdot}10^{-2}$	$6.42{\cdot}10^{-2}$
Final point	$4.48{\cdot}10^{-1}$	$7.11{\cdot}10^{-2}$	$1.68{\cdot}10^{-4}$	$1.53{\cdot}10^{-4}$

Table 2. Starting and final points of the optimization: design variables and OF values found with EStra-Many method

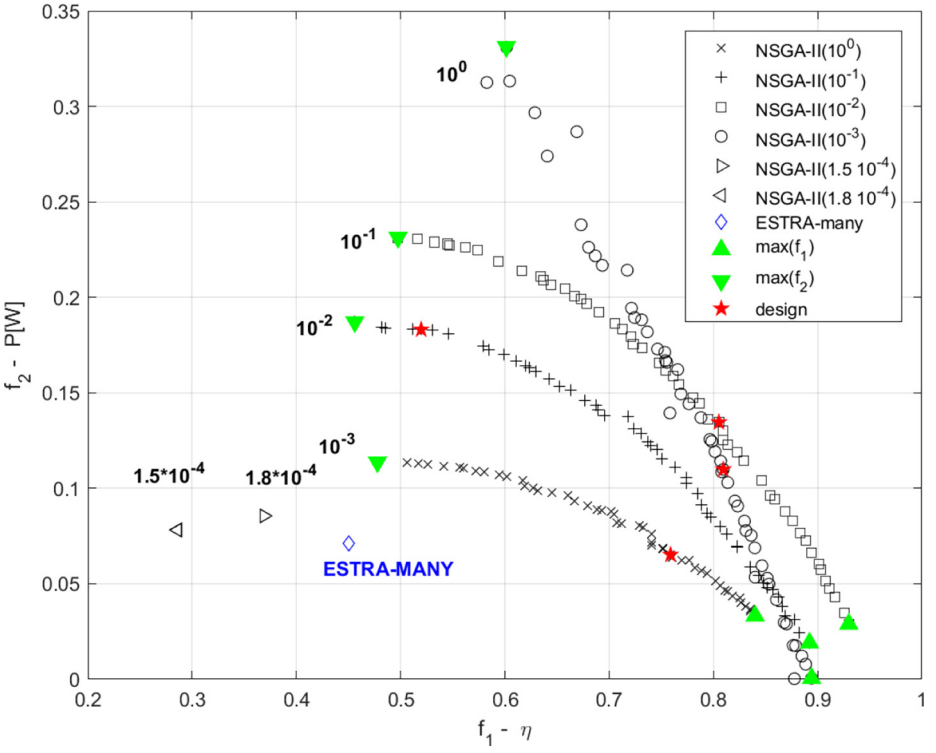

Figure 3. f_1–f_2 OF space with results of EStra-Many and NSGA-II (constrained bi-objective) methods

values of the OF f_1 and f_2 reached at the end of the optimization with constraints set to $1.5{\cdot}10^{-4}$ and $1.8{\cdot}10^{-4}$ are listed in Table 3.

It can be noted that these solutions are Pareto-indifferent with respect to the EStra-Many solution (blue diamond in Figure 3) because they worsen function f_1, whereas they are better for function f_2. This is also true if all the four OFs are considered at a time; for the sake of an example, let us consider Solutions 1 and 2 characterized by $k > 2$ OFs. It is enough that just one OF of Solution 1 is better than the corresponding OF of Solution 2, and another OF of Solution 1 is worse than the corresponding of Solution 2 that the two solutions are Pareto-indifferent. No matter the behavior of the remaining OFs.

Figure 4 shows the same Pareto fronts shown in Figure 3, but in Figure 4, the points are represented with different colors. Each color represents the range of values of the functions f_3 [Figure 4(a)] and f_4 [Figure 4(b)], which characterizes each solution. For instance, a green point in Figure 4(a) has an f_3 value between $10^{-2}<f_3<10^{-1}$, whereas a black point has $10^{-4}<f_3<10^{-3}$. The same colors are used to represent the range of values for f_4 in Figure 4(b).

Tables 4 and 5 show a selection of solutions related to constrained NSGA-II optimization considering different constraint levels for f_3 and f_4. The considered levels are $1.5{\cdot}10^{-4}$, $1.8{\cdot}10^{-4}$, 10^{-3}, 10^{-2}, 10^{-1} and 1. The selected solutions are those for which f_3 and f_4 are lower than $5{\cdot}10^{-4}$, respectively. It can be noted that even if f_3 and f_4 are constrained to be lower than a given threshold (e.g. 1), in the optimal solutions, f_3 and f_4 can assume lower values (e.g. close to 10^{-4}).

Table 6 shows a set of optimal solutions found with NSGA-II using four different constraint levels from 1 to 10^{-3}. In particular, the chosen solutions are those for which f_1 and f_2 are maximum, respectively (green triangles in Figure 3 and focus on point up and down, respectively) and others named design solutions, chosen *a posteriori* by the designer. These

Table 3.
Final points of the NSGA-II optimizations: design variables and OF values

	x_1 [Ω]	x_2 [Ω]	x_3 [Ω]	x_4 [Ω]	x_5 [Ω]	x_6 [Ω]
NSGA-II $1.5{\cdot}10^{-4}$	122.18	–375.32	–248.76	112.08	–82.62	125.35
NSGA-II $1.8{\cdot}10^{-4}$	119.96	–369.60	–246.21	108.72	–79.30	123.41
	η [NU]	**P_L [W]**	**$Z_{\omega 0}/Z_{\omega 100}$ (f_3 [NU])**		**$Z_{\omega 0}/Z_{\omega 0.01}$ (f_4 [NU])**	
NSGA-II 1.5 10^{-4}	0.286	$7.81{\cdot}10^{-2}$	$1.5{\cdot}10^{-4}$		$1.2{\cdot}10^{-4}$	
NSGA-II 1.8 10^{-4}	0.369	$8.55{\cdot}10^{-2}$	$1.8{\cdot}10^{-4}$		$1.5{\cdot}10^{-4}$	

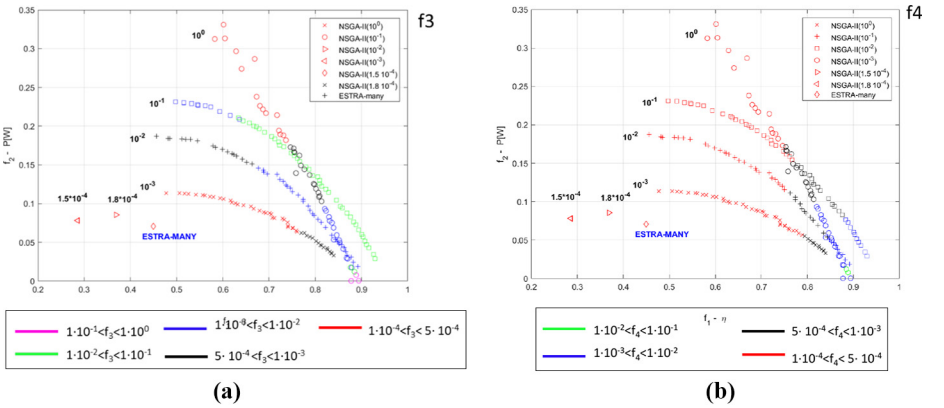

(a) (b)

Figure 4.
f_1–f_2 OF space with results of EStra-Many and NSGA-II methods

	x_1 [Ω]	x_2 [Ω]	x_3 [Ω]	x_4 [Ω]	x_5 [Ω]	x_6 [Ω]	η [NU]	PL [W]	f_3 [NU]	f_4 [NU]
EStra-Many	188	–380	–451	–57.2	–295	–22.4	0.448	0.0711	1.68·10–4	1.53·10–4
NSGA-II constraint level										
1·10^{0}	40	–56	–182	1	–471	–67	0.73	0.19	4.8·10^{-4}	4.5·10^{-4}
1·10^{-1}	NA									
1·10^{-2}	NA									
1·10^{-3}	NA									
1.8·10^{-4}	120	–370	–246	109	–79	123	0.37	0.09	1.8·10^{-4}	1.5·10^{-4}
1.5·10^{-4}	122	–375	–249	112	–83	125	0.29	0.08	1.5·10^{-4}	1.2·10^{-4}

Notes: NA: not available solution for the selected constraint level, NU: not unit

Table 4.
Improved solutions for which $f_3 < 5{\cdot}10^4$

solutions were chosen as a trade-off between f_1 and f_2 objectives, also considering the value of the function f_3 and f_4 and the shape of the Bode diagram of the impedance at the input of the WPTS. The chosen solutions show improved values for all four OFs.

Figure 5 shows the Bode diagram of the impedance $\overline{Z}_s$ (magnitude) at the terminals of the supply generator (Figure 1) for the solutions listed in Tables 2 and 3 obtained with EStra-Many and NSGA-II algorithms. In these diagrams, the fundamental harmonic at 85 kHz is denoted with the red circle, whereas the blue circles represent odd

Table 5.
Improved solutions for which $f_4 < 5{\cdot}10^{-4}$

	x_1 [Ω]	x_2 [Ω]	x_3 [Ω]	x_4 [Ω]	x_5 [Ω]	x_6 [Ω]	η [NU]	P_L [W]	f_3 [NU]	f_4 [NU]
EStra-Many	188	–380	–451	–57.2	–295	–22.4	0.448	0.0711	$1.68{\cdot}10^{-4}$	$1.53{\cdot}10^{-4}$
NSGA-II constraint level										
$\mathbf{1{\cdot}10^{0}}$	40	–57	–179	0	–470	–66	0.75	0.17	$5.3{\cdot}10^{-2}$	$5.0{\cdot}10^{-4}$
$\mathbf{1{\cdot}10^{-1}}$	2	–376	–62	–8	15	–11	0.77	0.15	$1.4{\cdot}10^{-2}$	$4.7{\cdot}10^{-4}$
$\mathbf{1{\cdot}10^{-2}}$	23	–226	–100	–86	–349	1	0.75	0.12	$1.4{\cdot}10^{-3}$	$4.7{\cdot}10^{-4}$
$\mathbf{1{\cdot}10^{-3}}$	124	–298	–282	–98	–49	18	0.76	0.06	$4.8{\cdot}10^{-4}$	$4.1{\cdot}10^{-4}$
$\mathbf{1.8{\cdot}10^{-4}}$	120	–370	–246	109	–79	123	0.37	0.09	$1.8{\cdot}10^{-4}$	$1.5{\cdot}10^{-4}$
$\mathbf{1.5{\cdot}10^{-4}}$	122	–375	–249	112	–83	125	0.29	0.08	$1.5{\cdot}10^{-4}$	$1.2{\cdot}10^{-4}$

Note: NU: not unit

Table 6.
Improved solutions for which f_1 and f_2 assume the maximum value, and the trade-off solutions at design point of view

Constr. level	Criteria	x_1 [Ω]	x_2 [Ω]	x_3 [Ω]	x_4 [Ω]	x_5 [Ω]	x_6 [Ω]	η [NU]	P_L [W]	f_3 [NU]	f_4 [NU]
10^{0}	max(f_1)	5	–500	–263	–30	–419	–36	0.894	0.001	$8.37{\cdot}10^{-3}$	$3.14{\cdot}10^{-1}$
10^{-1}	max(f_1)	2	–373	–64	–46	30	–13	0.930	0.029	$2.92{\cdot}10^{-3}$	$9.83{\cdot}10^{-2}$
10^{-2}	max(f_1)	23	–317	–104	–70	–349	1	0.892	0.019	$2.96{\cdot}10^{-3}$	$9.91{\cdot}10^{-3}$
10^{-3}	max(f_1)	126	–300	–281	–72	–66	7	0.840	0.033	$8.71{\cdot}10^{-4}$	$1.00{\cdot}10^{-3}$
10^{0}	max(f_2)	36	–43	–258	0	–471	–67	0.602	0.331	$2.45{\cdot}10^{-4}$	$2.51{\cdot}10^{-4}$
10^{-1}	max(f_2)	2	–375	–62	7	16	–6	0.497	0.231	$2.02{\cdot}10^{-4}$	$7.23{\cdot}10^{-3}$
10^{-2}	max(f_2)	22	–307	–93	–132	–349	18	0.456	0.187	$1.70{\cdot}10^{-4}$	$5.48{\cdot}10^{-4}$
10^{-3}	max(f_2)	118	–249	–288	–97	–26	21	0.478	0.114	$1.57{\cdot}10^{-4}$	$1.78{\cdot}10^{-4}$
10^{0}	design	41	–55	–211	–5	–468	–67	0.602	0.331	$2.45{\cdot}10^{-4}$	$2.51{\cdot}10^{-4}$
10^{-1}	design	1	–376	–61	–7	18	–13	0.805	0.135	$5.67{\cdot}10^{-4}$	$2.74{\cdot}10^{-2}$
10^{-2}	design	22	–308	–94	–124	–349	17	0.520	0.183	$1.97{\cdot}10^{-4}$	$6.34{\cdot}10^{-4}$
10^{-3}	design	124	–298	–283	–93	–36	16	0.759	0.065	$3.95{\cdot}10^{-4}$	$4.62{\cdot}10^{-4}$

Note: NU: not unit

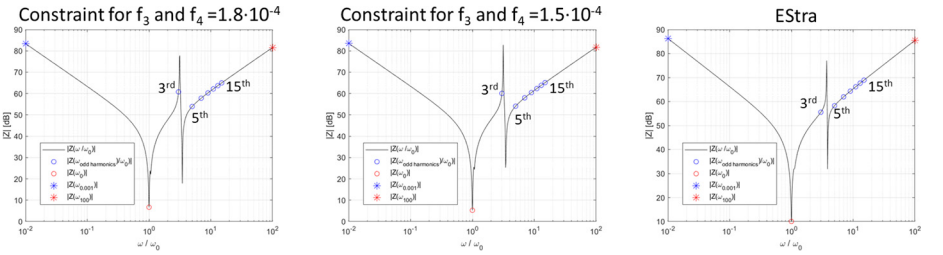

Figure 5.
Bode diagrams of the impedance at the output at the input of the WPTS obtained with EStra-Many algorithm and constrained NSGA-II algorithm (constraint level at $1.8{\cdot}10^{-4}$ and $1.5{\cdot}10^{-4}$)

harmonics from 3rd to 15th. The blue and red asterisk are set at $\omega=\omega_0/100$ and $\omega=\omega_0 \cdot 100$, respectively. The diagrams relevant to the solutions listed in Table 6 are reported in Figure 6 using the same meaning for the symbols.

The last comparison is performed between the EStra-Many solution, and the NSGA-II applied to four OFs. NSGA-II has been run with 50 individuals and 250 generations. The results are shown in Figure 7, where the projections of f_1 versus f_2, f_3 and f_4, respectively, and f_3 versus f_4 are shown. The EStra-Many solution is represented by means of a blue diamond, whereas the NSGA-II results are represented with crosses; the red crosses are solutions fulfilling the constraints $f_3<1$ or $f_4<1$, whereas the black crosses are unfeasible solutions.

After Figure 7, the following remarks can be put forward; the Estra-Many solution is located in the feasible region of the objective space i.e. in the region the red cross symbols belong to. Moreover, the Estra-Many solution is close to the NSGA-II solutions; this shows the capability of the proposed method to find a globally non-dominated solution. Hence, the two methods exhibit similar performance.

As far as the cost is concerned, we also note that EStra-Many finds one solution with 100–150 OF calls, whereas NSGA-II finds a set of 50 solutions with 250 generations i.e. up to $50 \times 250 = 6{,}250$ OF calls.

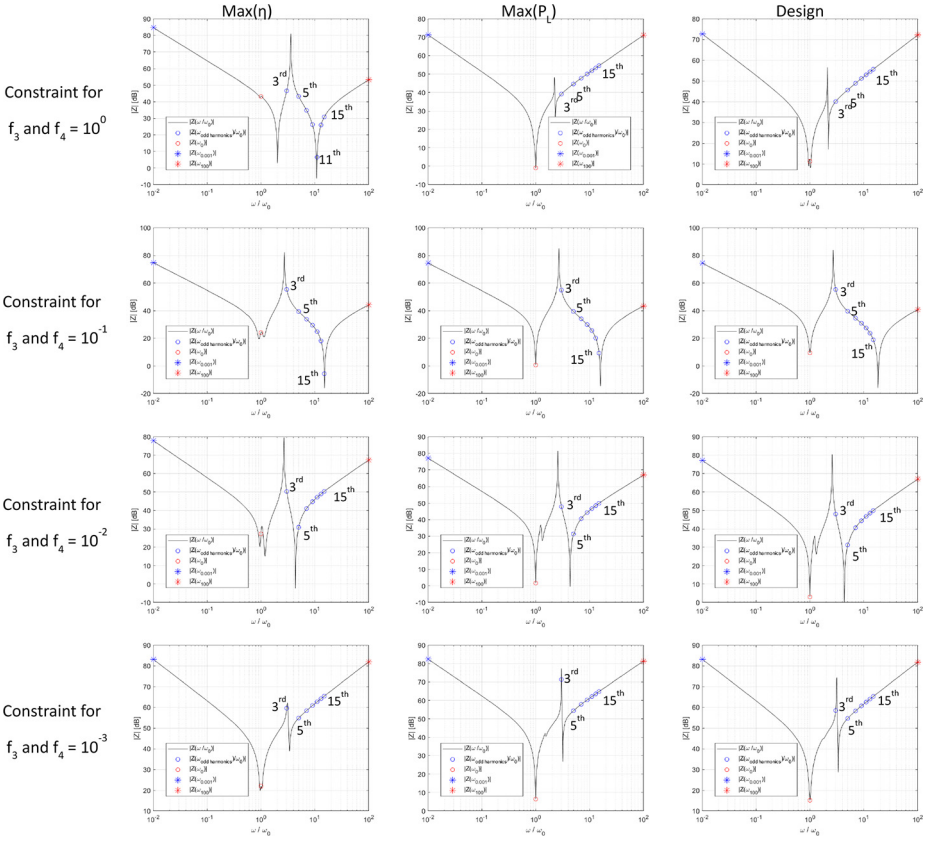

Figure 6.
Bode diagrams of the impedance of the WPTS obtained with constrained NSGA-II algorithm (constraint level between 10^{-3} and 10^{0})

5. Performance of the optimized compensation networks

The analysis Figures 5 and 6 allow drawing some general considerations about the behavior of the synthesized CNs. A common feature that appears in nearly all the diagrams is a resonance at the supply frequency ω_0. This characteristic is common also to conventional CNs, such as those built with the series-series or the series-parallel configurations. In fact, to maximize the transferred power with a given supply voltage, as the minimization of f_1 requires, the impedance at the output of the supply inverter must be minimized to obtain a high current. This remark helps also in explaining why the diagrams on the left column of Figure 6, characterized by low transferred power, have a poorly defined peak of resonance at ω_0, or no peak at all, like the first diagram.

Thanks to the requirement of minimizing both $Z_{\omega 0}/Z_{\omega 100}$ and $Z_{\omega 0}/Z_{\omega 0.01}$, all the diagrams exhibit a more or less defined wings-like shape and achieve high impedance values at high and low angular frequencies with respect to the supply one. Another common feature is the presence of a pair of spurious antiresonance-resonance peaks at angular frequencies higher than ω_0. The antiresonance peak is always set at a lower frequency than the resonance one, and their distance decreases as the requirements about the impedance ratios are tightened. It can also be found that when these requirements are loose, like it happens in the first two rows of Figure 6, some harmonics of the supply frequency are near to the spurious resonance peak, whereas in the other cases, they are far from it.

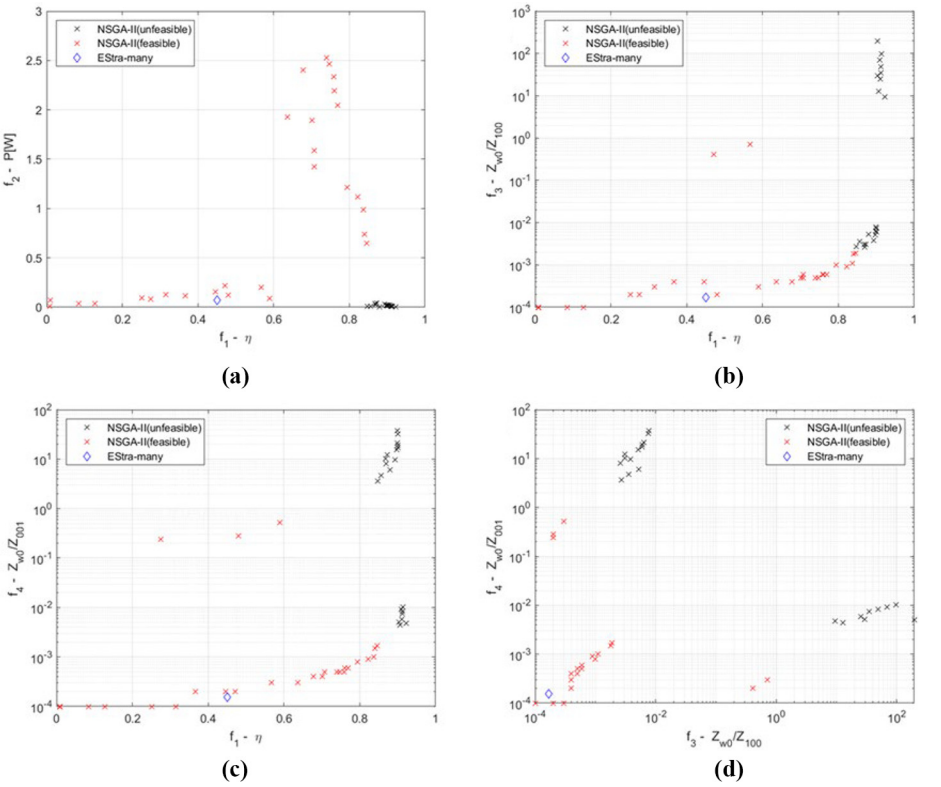

Figure 7.
OF space with results of EStra-Many and NSGA-II (multiobjective, four OFs) methods

To make easier the comparison between the optimized solution reached by EStra-Many and those found by NSGA-II, the three plots of Figure 5 have been superimposed to obtain Figure 8.

The red plot refers to the optimized solution obtained by EStra-Many and is characterized by the reactances listed in Table 2. The dashed blue and green plots are relevant to the optimized solutions reported in Table 3 and computed by NSGA-II. The parameters of the inductances and the equivalent load R_L used in computing the OFs are shown in Table 1. They are taken from a prototypal low-power WPTS device (Buja *et al.*, 2015).

The analysis of the plots in Figure 8 shows that both the optimization methods successfully prevent the flowing of unwanted current components in the supply inverter and in the transmitting CN. Indeed, for EStra-Many the ratios $Z_{\omega 0}/Z_{\omega 100}$ and $Z_{\omega 0}/Z_{\omega 0.01}$ are 75.5 dB and 72.9 dB, respectively, whereas for both the Bode diagrams relevant to NSGA-II, the ratios are 76.5 dB and 74.8 dB.

The pair of antiresonant-resonant peaks is between three and four times the supply frequency. From this point of view, EStra-Many provides better results than NSGA-II because the spurious resonance peaks have lower amplitude and are located at frequencies further away from the third harmonic of ω_0. Therefore, it is less likely that the resonance

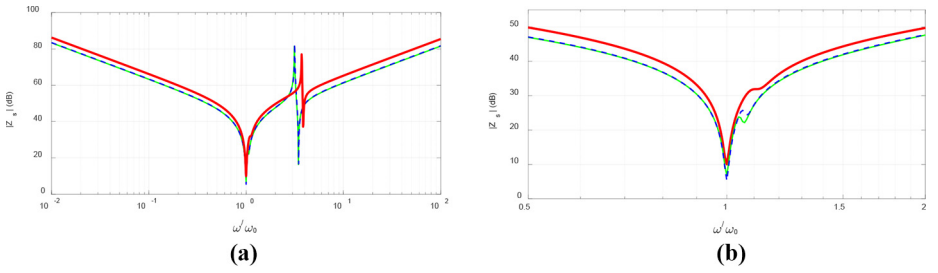

Figure 8.
Bode magnitude diagram of Z_s versus ω/ω_0 relevant to the optimized solutions obtained with EStra-Many and NSGA-II (a), magnification around the supply frequency (b)

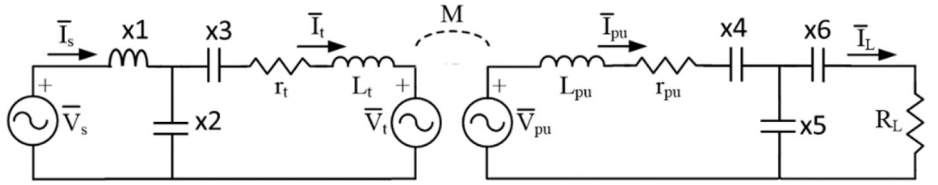

Figure 9.
Layout of the optimized CN obtained with EStra-Many algorithm

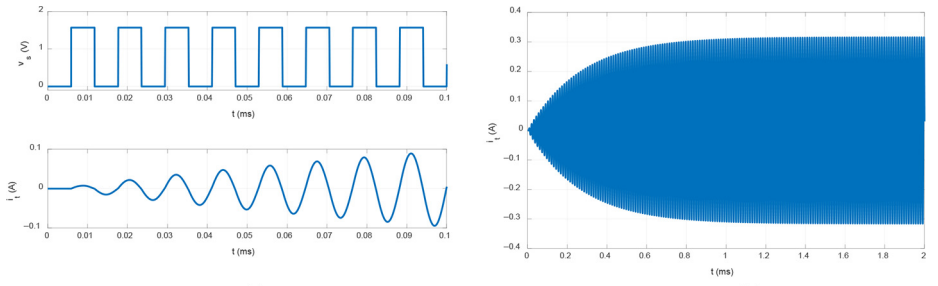

Figure 10.
Supply voltage (upper half) and supply current (lower half) during the first functioning periods (a), supply current from turning on to steady-state (b)

peaks affect the current of the supply inverter even if it generates a square wave voltage with a frequency a little higher than the nominal one. More precisely, the peak of minimum impedance coming from EStra-Many is set at a normalized frequency of 3.85 and has a magnitude of 37.19 dB, whereas both the peaks coming from NSGA-II are set at a normalized frequency of 3.47, and their magnitude is 16.45 dB, so that corresponding impedance is about 10 times lower than that obtained with EStra-Many.

At frequencies a little higher than the supply one, the Bode diagrams of the impedance exhibit a small distortion, as shown in Figure 8(b). Also, in this case, the solution coming from EStra-Many performs better than the other two because the distortion is smaller and happens at an angular frequency further away from the supply one.

A second verification of the optimization performance of EStra-Many has been carried out by a circuital simulation. Substituting in the circuit of Figure 1 the optimized values of the impedances, the circuit of Figure 9 has been obtained. It has been implemented in the Simulink environment to check the ability of the optimized CNs to reject both high and low-frequency components. To this end, the circuit has been supplied with a square-wave voltage with an offset equal to the voltage amplitude. The plot of the supply voltage is shown in the upper half of Figure 10(a). The waveform of the corresponding supply current is reported in the lower half of the same figure.

It clearly appears that the current does not exhibit any continuous component, and it is slightly distorted only in the very first supply periods while any harmonics disappear after a very short time interval. Figure 10(b) demonstrates that, despite the sudden application of the supply voltage, the current reaches smoothly its steady-state condition, without discontinuities or undue oscillations of its amplitude.

6. Conclusions

The comparison of the values taken by the OFs before and after the optimization shows that the EStra-Many algorithm effectively enhanced the performance of the CNs and their impedance to the unwanted current harmonics, as confirmed by the magnitude Bode diagram of Figure 7 and by the results coming from the simulations reported in Figure 9.

The EStra-Many method has been able to find a good solution among all the feasible solutions, showing potentiality also for other fields of research, in fact, a solution non-dominated with respect to the starting point has been identified. From the methodological viewpoint, the main finding is a new formulation of the many-objective optimization problem based on the concept of degree of conflict, which gives rise to an implementation free from hierarchical weights.

References

Ali, A., Sulaiman, M.I., Yasin, M.N.M., Azizan, M.M., Jusoh, M., Hambali, N.A.M.A. and Mat, M.H. (2019), "Wireless power transfer (WPT) optimization using resonant coil", *presented at the APPLIED PHYSICS OF CONDENSED MATTER (APCOM 2019)*, Strbske Pleso, Slovak Republic, p. 020127.

Ali, A., Mohd Yasin, M.N., Jusoh, M., Ahmad Hambali, N.A.M. and Abdul Rahim, S.R. (2020), "Optimization of wireless power transfer using artificial neural network: a review", *Microwave and Optical Technology Letters*, Vol. 62 No. 2, pp. 651-659.

Arduino, A., Bottauscio, O., Chiampi, M., Giaccone, L., Liorni, I., Kuster, N., Zilberti, L., *et al.* (2020), "Accuracy assessment of numerical dosimetry for the evaluation of human exposure to electric vehicle inductive charging systems", *IEEE Transactions on Electromagnetic Compatibility*, Vol. 62 No. 5, pp. 1939-1950.

Bertoluzzo, M. and Sieni, E. (2019), "Optimal design of the compensation networks of an inductive wireless power transfer system", *COMPEL – The International Journal for Computation and Mathematics in Electrical and Electronic Engineering*, Vol. 39 No. 1, pp. 231-238.

Bertoluzzo, M., Giacomuzzi, S. and Sieni, E. (2020), "Automatic optimization of the compensation networks of a wireless power transfer system", *Energies*, Vol. 13 No. 20, p. 5298.

Bertoluzzo, M., Forzan, M., Di Barba, P., Mognaschi, M.E. and Sieni, E. (2020), "Pareto optimal solutions of a wireless power transfer system", *The European Physical Journal Applied Physics*, Vol. 90 No. 2, p. 20904, edited by Razek, A.

Bi, Z., Kan, T., Mi, C.C., Zhang, Y., Zhao, Z. and Keoleian, G.A. (2016), "A review of wireless power transfer for electric vehicles: prospects to enhance sustainable mobility", *Applied Energy*, Vol. 179, pp. 413-425.

Buja, G., Bertoluzzo, M. and Mude, K.N. (2015), "Design and experimentation of WPT charger for electric city car", *IEEE Transactions on Industrial Electronics*, Vol. 62 No. 12, pp. 7436-7447.

Campi, T., Cruciani, S., Maradei, F. and Feliziani, M. (2020), "Magnetic field mitigation by multicoil active shielding in electric vehicles equipped with wireless power charging system", *IEEE Transactions on Electromagnetic Compatibility*, Vol. 62 No. 4, pp. 1398-1405.

Chen, W., Lu, W., Iu, H.H.-C. and Fernando, T. (2020), "Compensation network optimal design based on evolutionary algorithm for inductive power transfer system", *IEEE Transactions on Circuits and Systems I: Regular Papers*, Vol. 67 No. 12, pp. 5664-5674.

Choi, S.Y., Gu, B.W., Jeong, S.Y. and Rim, C.T. (2015), "Advances in wireless power transfer systems for Roadway-Powered electric vehicles", *IEEE Journal of Emerging and Selected Topics in Power Electronics*, Vol. 3 No. 1, pp. 18-36.

Cirimele, V., Diana, M., Freschi, F. and Mitolo, M. (2018), "Inductive power transfer for automotive applications: state-of-the-Art and future trends", *IEEE Transactions on Industry Applications*, Vol. 54 No. 5, pp. 4069-4079.

Covic, G.A. and Boys, J.T. (2013a), "Inductive power transfer", *Proceedings of the IEEE*, Vol. 101 No. 6, pp. 1276-1289.

Covic, G.A. and Boys, J.T. (2013b), "Modern trends in inductive power transfer for transportation applications", *IEEE Journal of Emerging and Selected Topics in Power Electronics*, Vol. 1 No. 1, pp. 28-41.

Cruciani, S., Campi, T., Maradei, F. and Feliziani, M. (2020a), "Active shielding design and optimization of a wireless power transfer (WPT) system for automotive", *Energies*, Vol. 13 No. 21, p. 5575.

Cruciani, S., Campi, T., Maradei, F. and Feliziani, M. (2020b), "Active shielding applied to an electrified road in a dynamic wireless power transfer (WPT) system", *Energies*, Vol. 13 No. 10, p. 2522.

D'Souza, R., Sekaran, C. and Kandasamy, A. (2010), "Improved NSGA-II based on a novel ranking scheme", *Journal of Computing*, Vol. 2.

Deb, K. and Jain, H. (2014), "An evolutionary Many-Objective optimization algorithm using Reference-Point-Based nondominated sorting approach, part I: solving problems with box constraints", *IEEE Transactions on Evolutionary Computation*, Vol. 18 No. 4, pp. 577-601.

Deb, K. (2001), *Multiobjective Optimization Using Evolutionary Algorithms*, 1st ed., John Wiley and Sons, Chichester ; New York, NY.

Di Barba, P. and Mognaschi, M.E. (2009), "Industrial design with multiple criteria: shape optimization of a Permanent-Magnet generator", *IEEE Transactions on Magnetics*, Vol. 45 No. 3, pp. 1482-1485.

Di Barba, P., Mognaschi, M.E. and Wiak, S. (2020), "A non-differential method for solving many-objective optimization problems: an application in IPM motor design", *International Journal of Applied Electromagnetics and Mechanics*, Vol. 64 No. S1, pp. S131-S142.

Di Capua, G., Femia, N., Stoyka, K., Di Mambro, G., Maffucci, A., Ventre, S. and Villone, F. (2021), "Mutual inductance behavioral modeling for wireless power transfer system coils", *IEEE Transactions on Industrial Electronics*, Vol. 68 No. 3, pp. 2196-2206.

Feng, H., Cai, T., Duan, S., Zhang, X., Hu, H. and Niu, J. (2018), "A Dual-Side-Detuned series–series compensated resonant converter for wide charging region in a wireless power transfer system", *IEEE Transactions on Industrial Electronics*, Vol. 65 No. 3, pp. 2177-2188.

Jha, R.K., Buja, G., Bertoluzzo, M., Giacomuzzi, S. and Mude, K.N. (2018), "Performance comparison of the One-Element resonant EV wireless battery chargers", *IEEE Transactions on Industry Applications*, Vol. 54 No. 3, pp. 2471-2482.

Kindl, V., Frivaldsky, M., Zavrel, M. and Pavelek, M. (2020), "Generalized design approach on industrial wireless chargers", *Energies*, Vol. 13 No. 11, p. 2697.

Lahanas, M., Schreibmann, E., Milickovic, N. and Baltas, D. (2003), *Evolutionary Multi-Criterion Optimization*, Vol. 2632, Springer, Berlin/Heidelberg, p. 70.

Lee, S.B., Ahn, S., Lee, J.H. and Jang, I.G. (2014), "Optimization of the wireless power transfer system in an electric railway", *2014 IEEE Wireless Power Transfer Conference, presented at the 2014 IEEE Wireless Power Transfer Conference (WPTC)*, IEEE, *Jeju City, South Korea*, pp. 158-161.

Li, W., Zhao, H., Li, S., Deng, J., Kan, T. and Mi, C.C. (2015), "Integrated LCC compensation topology for wireless charger in electric and plug-in electric vehicles", *IEEE Transactions on Industrial Electronics*, Vol. 62 No. 7, pp. 4215-4225.

Li, Y., Hu, J., Chen, F., Li, Z., He, Z. and Mai, R. (2018), "Dual-Phase-Shift control scheme with Current-Stress and efficiency optimization for wireless power transfer systems", *IEEE Transactions on Circuits and Systems I: Regular Papers*, Vol. 65 No. 9, pp. 3110-3121.

Lukic, S. and Pantic, Z. (2013), "Cutting the cord: static and dynamic inductive wireless charging of electric vehicles", *IEEE Electrification Magazine*, Vol. 1 No. 1, pp. 57-64.

Mohamed, A.A.S., Berzoy, A., de Almeida, F.G.N. and Mohammed, O. (2016), "Steady-state performance assessment of different compensation topologies in two-way IWPT system for EV ancillary services", *2016 IEEE Industry Applications Society Annual Meeting, presented at the 2016 IEEE Industry Applications Society Annual Meeting*, IEEE, *Portland, OR, USA*, pp. 1-8.

Orasanu, A., Dragomir, A., Bobaru, L., Iordache, M. and Deleanu, S. (2018), "On optimization of wireless power transfer systems", *2018 International Symposium on Fundamentals of Electrical Engineering (ISFEE), presented at the 2018 International Symposium on Fundamentals of Electrical Engineering (ISFEE)*, IEEE, *Bucharest, Romania*, pp. 1-6.

Pantic, Z. and Lukic, S.M. (2012), "Framework and topology for active tuning of parallel compensated receivers in power transfer systems", *IEEE Transactions on Power Electronics*, Vol. 27 No. 11, pp. 4503-4513.

Qingfu Zhang, H.L. (2009), "Multiobjective optimization problems with complicated pareto sets, MOEA/D and NSGA-II", *Evolutionary Computation, IEEE Transactions On*, Vol. 13 No. 2, pp. 284-302.

Qu, X., Jing, Y., Han, H., Wong, S.C. and Tse, C.K. (2017), "Higher order compensation for Inductive-Power-Transfer converters with Constant-Voltage or Constant-Current output combating transformer parameter constraints", *IEEE Transactions on Power Electronics*, Vol. 32 No. 1, pp. 394-405.

Shen, S. and Clerckx, B. (2021), "Joint waveform and beamforming optimization for MIMO wireless power transfer", *IEEE Transactions on Communications*, Vol. 69 No. 8, pp. 5441-5455.

Siqi, L. and Mi, C.C. (2015), "Wireless power transfer for electric vehicle applications", *IEEE Journal of Emerging and Selected Topics in Power Electronics*, Vol. 3 No. 1, pp. 4-17.

Tan, L., Zhang, M., Wang, S., Pan, S., Zhang, Z., Li, J. and Huang, X. (2019), "The design and optimization of a wireless power transfer system allowing random access for multiple loads", *Energies*, Vol. 12 No. 6, p. 1017.

Villa, J.L., Sallan, J., Sanz Osorio, J.F. and Llombart, A. (2012), "High-Misalignment tolerant compensation topology for ICPT systems", *IEEE Transactions on Industrial Electronics*, Vol. 59 No. 2, pp. 945-951.

Winges, J., Rylander, T., Petersson, C., Ekman, C., Johansson, L.-A. and McKelvey, T. (2019), "Multiobjective optimization of wireless power transfer systems with magnetically coupled resonators and nonlinear loads", *Progress in Electromagnetics Research B*, Vol. 83, pp. 25-42.

Yakala, R.K., Pramanick, S., Nayak, D.P. and Kumar, M. (2021), "Optimization of circular coil design for wireless power transfer system in electric vehicle battery charging applications", *Transactions of the Indian National Academy of Engineering*, Vol. 6 No. 3, pp. 765-774.

Zhang, W. and Mi, C.C. (2016), "Compensation topologies of High-Power wireless power transfer systems", *IEEE Transactions on Vehicular Technology*, Vol. 65 No. 6, pp. 4768-4778.

Further reading

SAE (n.d.). "SAE J 2954 wireless power transfer for Light-Duty plug-in/electric vehicles and alignment methodology", available at: www.sae.org/standards/content/j2954_201605/

Corresponding author

Maria Evelina Mognaschi can be contacted at: eve.mognaschi@unipv.it